RSC Advances

PAPER

View Article Online
View Journal | View Issue

Cite this: *RSC Adv.*, 2026, **16**, 15225

Removal of ciprofloxacin from aqueous solutions using GO/PVA/calcium alginate composite beads as an absorbent

Md. Samrat Hossain, Md. Anwarul Karim * and Sharmin Sultana Dipti

We prepared an eco-friendly graphene oxide (GO)-incorporated composite bead adsorbent, comprising sodium alginate (SA) and polyvinyl alcohol (PVA), *via in situ* cross-linking between GO and SA using calcium chloride as a cross-linking reagent, which is uniformly distributed within the PVA matrix. Fourier transform infrared (FTIR) spectroscopic analysis of the functional groups confirmed the successful preparation of the composite. The batch process was used to treat aqueous solutions containing CPX. Adsorbent characteristics are evaluated through measurements of moisture content, ash content, point of zero charge (pHpzc), pore volume, ion exchange capacity, specific surface area, oxidative stability, thermogravimetric analysis (TGA), X-ray diffraction (XRD), scanning electron microscopy (SEM), energy-dispersive spectroscopy (EDS), and X-ray spectroscopy. The point of zero charge, specific surface area, moisture content, ash content, pore volume, ion exchange capacity, and oxidative stability of the adsorbent were 7.07, 1991 mg g^{-1}, 11.72%, 78.92%, 1.7%, 0.7857%, and 96.45%, respectively. Adsorption experiments revealed that the beads achieved the maximum adsorption capacity under optimal conditions and that the highest removal efficiency was 89.82%. Among the four linear and non-linear isotherms, the Langmuir adsorption isotherm model indicated that the adsorption occurred by monolayer formation. Thermodynamic and kinetic analyses indicate that the adsorption process is spontaneous and exothermic, and that it adheres to pseudo-second-order kinetics. These findings highlight the GO/PVA/CA composite beads as promising, economical, and eco-friendly adsorbents for the removal of pharmaceutical contaminants (especially CPX) from wastewater.

Received 19th January 2026
Accepted 1st March 2026

DOI: 10.1039/d6ra00494f

rsc.li/rsc-advances

1. Introduction

Wastewater from the pharmaceutical, aquaculture, and animal husbandry industries is the primary contributor to antibiotic contamination.[1] The human body, along with animals and plants, absorbs and metabolizes antibiotic medicines. Subsequently, these substances are eliminated from the body as precursor compounds or metabolites, which are then disposed of as solid waste in sewage systems.[2–6] Recent studies indicate that approximately 80% of antibiotics administered in livestock and aquaculture operations are released into aquatic environments or settle to the bottom along with feed, urine, and dung. Pharmaceutical and medical wastewaters are characterized by significant biological toxicity,[7–12] a high concentration of antibiotics, and considerable fluctuations in the concentration and water volume.[13] Conventional wastewater treatment methods often fail to remove antibiotics effectively. Consequently, sludge or processed wastewater is often released into the environment, accompanied by undecomposed drugs.[14,15] Furthermore, a major contributing factor to the high levels of antibiotics in the ecosystem is the improper disposal of expired antibiotics.[16,17]

Ciprofloxacin (CPX) [$C_{17}H_{18}FN_3O_3$] is a synthetic quinolone classified as a third-generation antibiotic, widely recognized for its potent antimicrobial activity. However, CPX is known for its difficulty in biodegradation.[18] There are three distinct forms of CPX in a solution: cationic, characterized by the amino group (has a charge of +1) in solutions with a pH of less than 5.90 ± 0.15; anionic, which has a carboxylate anion (hydrogen ions, H^+, removed from it) in solutions with a pH greater than 8.89 ± 0.11; and zwitterionic, which has positively (cationic form) and negatively (anionic form) charged functional groups, as shown in Fig. 1, resulting in an overall neutral charge.[19] CPX may enter aquatic habitats through manufacturing processes or as partially metabolized substances excreted by humans.[20] At high concentrations, CPX can weaken the immune system and promote the proliferation of antibiotic-resistant bacteria.[21]

This scenario can foster a vicious cycle, in which more resilient bacterial infections require increasing doses of CPX for treatment. This vicious cycle may result in elevated CPX concentrations in the environment, which can be extremely harmful to human health. Consequently, before release, CPX levels must be brought within appropriate limits.[22]

Department of Applied Chemistry and Chemical Engineering, University of Rajshahi, Motihar, Rajshahi 6205, Bangladesh. E-mail: makarim72@ru.ac.bd

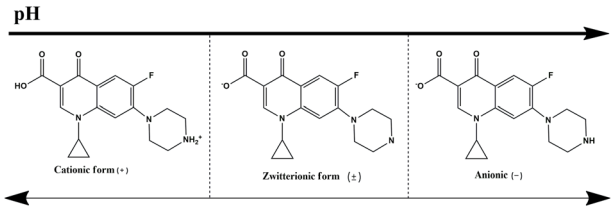

Fig. 1 The pH-dependent three-ionization form of CPX.

Many techniques, such as membrane separation,[23] oxidation reactions,[24] adsorption treatment,[18] activated sludge treatment,[25] microbial degradation,[26] and photocatalytic degradation,[27] have been used to extract CPX from wastewater; among them, some are chemical and physical methods. Adsorption treatment is considered the most promising of these techniques due to its simple theoretical design, cost-effectiveness, ease of use, and relatively minimal creation of hazardous byproducts.[28–30] A variety of adsorbents, including activated carbon,[31] montmorillonite,[32] carbon nanotubes,[33] hydrous iron oxides,[32] kaolinite,[33] and graphene,[34] have been investigated for the removal of CPX from aqueous solutions.

Sodium alginate (SA), the sodium salt of alginic acid, comprises copolymers that feature β-1,4-glycosidic linkages between β-L-mannuronic acid (unit M) and β-D-guluronic acid (unit G).[35] Due to its biocompatibility, nontoxicity and abundance of hydroxyl and carboxyl groups, SA readily interacts with polyvalent ions such as Ba^{2+}, Ca^{2+}, and Fe^{3+}, facilitating cross-linking. This characteristic has led to the use of SA as an adsorbent for the removal of heavy metals,[36] dyes,[37] and antibiotics.[33] The pore structure of the SA gel plays a vital role in the adsorption process in these studies. However, these solutions and gels are also susceptible to bacterial contamination.[38] To enhance adsorption capacities and impart antibacterial properties, numerous studies have focused on improving the structure of the alginate pores.[39–41]

With its two-dimensional, sheet-like carbon structure, graphene oxide (GO) has become one of the most popular carbon compounds in recent years. Its surface and borders are sporadically decorated with carboxyl, epoxy, and hydroxyl groups. These features enable cation interactions, hydrogen bonding, π–π stacking, and other special mechanical and physicochemical capabilities. They also provide a significant specific surface area and exceptional dispersibility in aqueous solutions.[42] GO and its compounds have been proven to be effective in the removal of various contaminants, including methyl blue,[43] tetracycline antibiotics,[44] arsenic,[45] and Hg^{2+}.[46] However, the application of GO in environmental contexts is somewhat limited due to its potential nanotoxicity.[47] Furthermore, it is challenging for GO to adsorb antibiotics effectively.

Recent studies on wastewater treatment have focused a lot of interest on graphene and graphene oxide (GO) because of their exceptional ability to adsorb a variety of pollutants. In this study, we utilized sol–gel chemistry to fabricate novel GO/PVA/CA hybrid composite gel beads by encapsulating graphene oxide in sodium alginate (SA). This method enhanced the pore uniformity of sodium alginate, reduced average pore size, and mitigated the nanotoxicity associated with GO. The gel beads were characterized using thermogravimetric analysis (TGA), focused ion beam scanning electron microscopy (SEM), and Fourier transform infrared (FT-IR) spectroscopy. Investigations on CPX adsorption were conducted by taking into account the effects of the adsorbent dosage, agitation time, and initial CPX concentration. The equilibrium adsorption data were fitted to nonlinear Langmuir isotherms to ascertain the composites' maximum adsorption capabilities. Furthermore, pseudo-first-order and pseudo-second-order kinetics models were used to assess the adsorption kinetics.

2. Materials and methods

2.1. Materials

CPX was collected from Square Pharmaceuticals Ltd, Bangladesh. Sodium alginate (SA), polyvinyl alcohol (PVA), boric acid (H_3BO_3), anhydrous calcium chloride ($CaCl_2$, MW = 110.98 g mol^{-1}) and a fine graphite powder (98% extra pure) were purchased from Chinese Sinopharm Chemical Reagent Co., Ltd. Potassium permanganate ($KMnO_4$, MW = 158.83 g mol^{-1}), 30% hydrogen peroxide, 37% hydrochloric acid, 98% sulfuric acid, and phosphoric acid (H_3PO_4) were obtained from BDH Chemicals Limited, UK. All chemicals were used without further purification.

2.2. Preparation of graphene oxide using a modified Hummers' method

Graphene oxide was produced by the modified Hummers' process using the graphite powder.[48] In this method, phosphoric acid and sulfuric acid were mixed in a 1 : 9 volume ratio (we used 170.2 mL of H_2SO_4 and 19.4 mL of H_3PO_4 for a 200 mL batch) and stirred for several minutes in an ice bath. 1 g of the graphite powder and 9.8 g of potassium permanganate ($KMnO_4$) were gradually introduced into 200 mL of the mixed solution under stirring, as shown in Fig. 2. The mixture was transferred to an oil bath and heated at 90 °C for 90 minutes. After adding 75 mL of deionized water, the mixture was stirred and left for 120 minutes. The reaction was then stopped by gradually adding 40 mL of hydrogen peroxide and 125 mL of deionized water (DI) while the mixture was submerged in an ice bath. It was

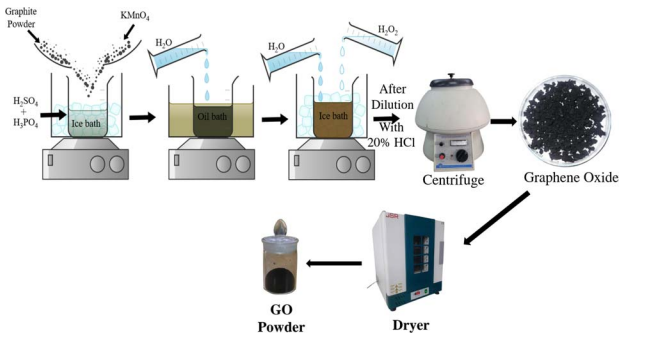

Fig. 2 Preparation of the GO/PVA/CA composite.

necessary to chill the solution because an exothermic reaction had occurred. A centrifuge machine (DSC-200A-2) was used to centrifuge the resulting solution for 20 minutes at 6000 rpm after it was diluted with a 20% HCl solution. After removing the supernatant, the precipitates were washed repeatedly with deionized (DI) water until a neutral pH was achieved. The samples produced were then dried for around 36 hours at 100 °C in an oven.

2.3. Preparation of GO/PVA/CA composite beads

A homogeneous GO/water solution was prepared by ultrasonically dispersing 0.5 g and 1 g of GO separately in 100 mL of deionized water for 60 minutes at room temperature. Subsequently, 5 g of PVA was added to the mixture, which was then stirred at 85 °C until it was fully dissolved. Then, at 65 °C, 5 g of SA was added to the mixture and stirred until it was fully dissolved.

After 3 hours of sonication to create a homogeneous solution, the solution was degassed. After cooling, the GO/PVA/CA dispersion was added dropwise into a mixed curing solution containing saturated boric acid (5%) and $CaCl_2$ (5%) using a peristaltic pump (15 rpm, 1 mm internal pipe diameter). The solution was then carefully stirred to create spherical hydrogel beads, as shown in Fig. 2. Finally, to achieve a stable shape, the gel beads were submerged in a $CaCl_2$-saturated boric acid mixed solution for 12 hours. The graphical representation of the chemical reaction that occurs during the preparation of GO/PVA/CA is presented in Fig. 3.

2.4. Characterization

The structural analysis of the GO powder and GO/PVA/CA composite bead samples was performed with an FTIR spectrometer (Nicolet-560, USA) within the range of 4000–400 cm^{-1}.

The crystallinity of the GO/PVA/CA samples was analyzed using an X-ray diffractometer (Tokyo, Japan). The Bragg equation was used to calculate the d-spacing of the GO samples:

$$2d \sin \theta = n\lambda \quad (1)$$

where n is the order of diffraction, λ is the incident wavelength, and θ is the angle of diffraction.

The TGA PerkinElmer simultaneous thermal analyzer (STA) 8000 was used to study the thermal stability of the GO/PVA/CA composite bead adsorbents. Heat was applied at 20 °C min^{-1}, and the temperature range was from 15 °C to 800 °C.

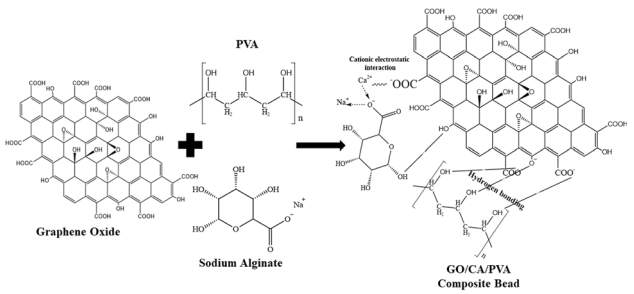

Fig. 3 Chemical reaction involved in the synthesis of the GO/PVA/CA composite preparation.

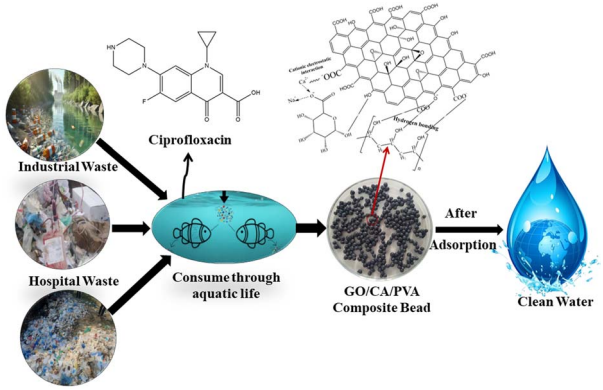

Fig. 4 Illustration of the purification process for the removal of CPX from the aqueous solution.

At an operating voltage of 15 kV, the surface morphologies of the GO/PVA/CA composite hydrogel beads were examined using SEM (Tokyo, Japan). After being cryogenically shattered in liquid nitrogen and freeze-dried, the samples were sputter-coated with gold for 4 minutes.

To analyze the elemental composition of the composite, EDS was used in combination with scanning electron microscopy (SEM). When a material is bombarded with an electron beam, it emits X-rays, each corresponding to a specific energy that is unique to the element present in the sample. By measuring these X-rays, EDS can identify and quantify the elements in the sample. The expected mechanism of purification of CPX-contaminated wastewater is shown in Fig. 4.

3. Results and discussion

3.1. The properties of the GO/PVA/CA composite bead

In a standard procedure,[49–52] 30.0 mL of a 0.1 M NaCl solution was added to a conical flask along with 30 mg of the GO/PVA/CA composite beads. When necessary, 0.1 M HCl and 0.1 M NaOH were used to bring the pH down to the appropriate value of 2, 3, 4, 5, 6, 7, 8, 9, 10, and 11 (±0.1 pH units). The pH level was used to represent the supernatant values in each conical flask. The sample was shaken at 200 rpm for 24 hours. After settling, the pH values of the supernatant in each conical flask were measured and recorded as pH, as illustrated in Fig. 5.

The pHpzc was obtained from the plot of ΔpH against pH.

$$\Delta pH = (pH_i - pH_f) \quad (2)$$

Here, the point of zero charge value is measured as 7.07.

3.2. Adsorption mechanisms

The adsorption of ciprofloxacin (CPX), a fluoroquinolone antibiotic, onto graphene oxide/polyvinyl alcohol/calcium alginate (GO/PVA/CA) composite beads involves multiple interaction mechanisms driven by the composite's functional groups and structure. These beads combine GO's high surface area and π–π

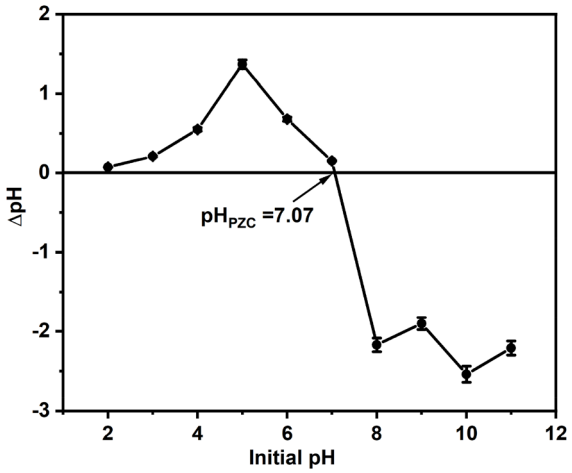

Fig. 5 Point of zero charge value of the GO/PVA/CA composite beads.

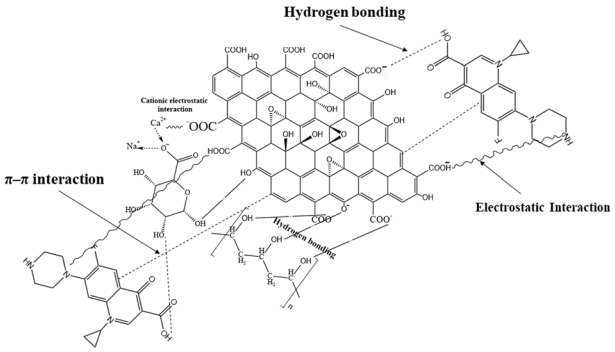

Fig. 6 CPX adsorption mechanism on the GO/PVA/CA composite bead surface.

stacking sites, PVA's hydrogen bonding capability, and CA's ion-exchange properties for enhanced removal of CPX from aqueous solutions.[53] The process by which CPX is adsorbed onto GO/PVA/CA composite beads is shown in Fig. 6.

At the optimal pH, CPX's protonated amine and zwitterionic carboxyl groups interact with GO's negatively charged sites (carboxyl groups) and alginate's guluronate blocks, favouring cation exchange with Ca^{2+}.[22] The hydroxyl (–OH) and carboxyl (–COOH) groups on GO, PVA, and alginate form H-bonds with CPX's fluoroquinolone ring, amine, and carbonyl oxygens, boosting affinity under neutral conditions.[53] This is in agreement with the point of zero charge value of the GO/PVA/CA composite beads, as shown in Fig. 5. The GO's aromatic graphene sheets enable π–π stacking with CPX's quinolone rings, while PVA enhances bead stability and hydrophilicity to prevent aggregation.[54] Graphene oxide (GO) improves the pore uniformity and surface area of polyvinyl alcohol/calcium alginate (PVA/CA) beads through ionic crosslinking, while PVA contributes to enhanced mechanical stability. Analogous composites, such as GO–sodium alginate (GO–SA) beads, demonstrate a 7–9-fold increase in capacity compared to pure or only alginate. The measured properties of the GO/PVA/CA composite beads are summarized in Table 1.

Table 1 Proximate analysis of the GO/PVA/CA composite bead as an adsorbent

Measurement	Value
Specific surface area	1991 mg g^{-1}
Moisture content	11.72%
Pore volume	78.92%
Ash content	1.7%
Ion exchange capacity (IEC)	0.7857 meq. per g
Oxidative stability	96.45%

3.3. FTIR study

In this study, the infrared spectra of the GO/PVA/CA composite were analyzed before and after CPX adsorption. The FTIR spectra are presented in Fig. 7. The GO spectrum exhibits many well-known peaks due to the presence of oxygenated groups, including –OH, –COOH, and C=O (ketone) groups, among others. The unique peaks associated with the stretching vibrations of –OH (3429 cm^{-1}), –COOH (1725 cm^{-1}), –C=C– (1629 cm^{-1}), and C–OH (1069 cm^{-1}) indicate the presence of oxygen on flat, two-dimensional graphene oxide (GO).[55–57] The stretching vibrations of the epoxy groups (C–OC) and C–OH groups, respectively, are identified as the cause of the absorption peaks at 1069 cm^{-1} and 1254 cm^{-1}, respectively. The appearance of distinctive absorption peaks associated with PVA and SA molecules, such as the one at 1425 cm^{-1}, which corresponds to the COO^- stretching vibration, and those at 1069 and 889 cm^{-1}, which are attributed to the stretching vibrations of OH and C–C, respectively, suggests that the PVA and SA molecules are intercalated into GO layers through hydrogen bonding interactions.

3.4. Thermogravimetric analysis

TGA was used to perform a thermal investigation of the GO/PVA/CA adsorbent before and after CPX adsorption, as shown

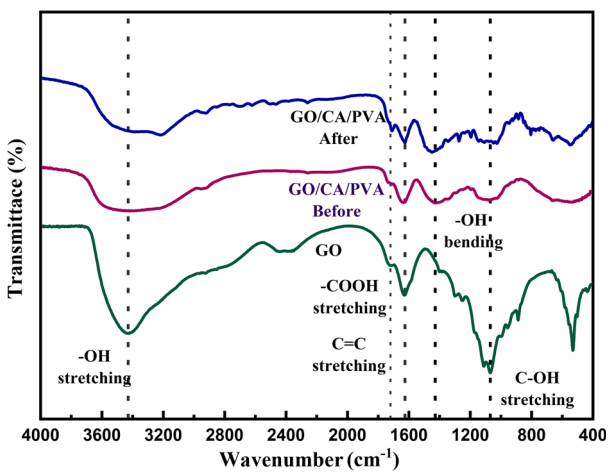

Fig. 7 FTIR spectra of GO, the GO/PVA/CA composite before CPX adsorption, and the GO/PVA/CA composite after the adsorption of CPX.

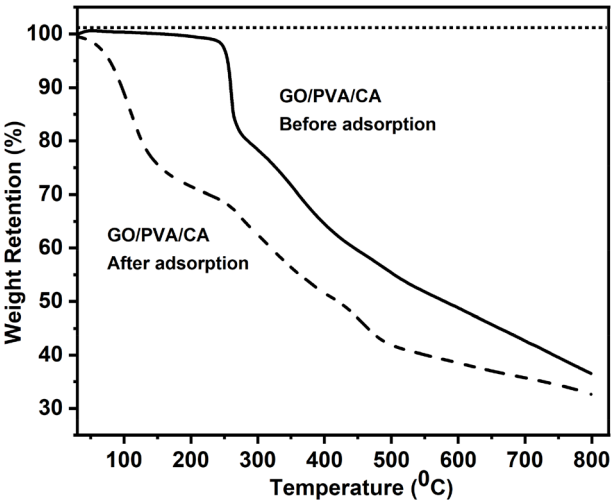

Fig. 8 Thermogravimetric analysis (TGA) of the GO/PVA/CA composite beads before and after the adsorption of CPX.

in Fig. 8. The TGA graph shows the first weight loss in the temperature range between 100 °C and 150 °C, corresponding to the evaporation of bound water absorbed within the composite beads. The breakdown of the functional groups causes a further weight decrease in the TGA graph between 250 °C and 300 °C before adsorption. In this area, the weight loss is more pronounced for composite beads due to the higher number of functional groups on the surface of graphene oxide (GO). On the contrary, the fluctuation in the weight loss is more pronounced in the range from 300 °C to 700 °C. This is due to the rapid and extensive combustion of the polymer, which results in a residual stable hybrid composite that includes GO. The ultimate disintegration occurs as a result of the degradation of the polymer backbone. The third stage occurs around 750 °C, and the TGA spectrum shows that the breakdown occurs over a wider temperature range than for the GO/PVA/CA composite beads because it contains thermally stable graphene oxide. After adsorption, the interaction between the functional groups and CPX diminishes in the second stage, resulting in a weight loss in the TGA graph between 150 °C and 250 °C, as shown in Fig. 8. The weight loss consistently decreases as the temperature increases.

3.5. Adsorption capacity and removal efficiency

CPX aqueous stock solutions with known concentrations were prepared. Adsorption experiments with CPX were performed using a batch process. Specific amounts of CPX-containing solutions were added to a conical flask, and specific amounts of the GO/PVA/CA composite adsorbent beads were added.[58] The samples were then shaken at 200 rpm at a fixed temperature. After the contact time, the samples were centrifuged at 5000 rpm to separate the adsorbent from the solution. To determine the optimal conditions for adsorption, the experiments were carried out by changing the adsorbent dose (0.1–0.5 g), concentration (20, 40, 60, 80, and 100 mg L^{-1}), pH (4–10), contact time (30–180 min), and temperature (30 °C, 40 °C, 50 °C, 60 °C, and 70 °C). The pH of the solutions was adjusted by adding 0.1 M HCl or 0.1 M NaOH until a suitable pH was achieved. The final concentration of each sample was calculated using UV-vis spectroscopy at a wavelength of 274 nm.[54,59] The percentage of removal of the GO/PVA/CA composite beads was calculated as follows:[22,60,61]

$$\text{Removal percentage } (\%\ R) = \frac{C_0 - C_t}{C_0} \times 100 \quad (3)$$

The adsorption capacity at equilibrium (q_e) and the adsorption capacity at time t (q_t) of the GO/PVA/CA composite beads were calculated as follows:

$$q_e = \frac{C_0 - C_e}{M} \times V \quad (4)$$

where C_0 and C_e are the initial and final concentrations (mg mL^{-1}) of antibiotics, respectively.

$$q_t = \frac{C_0 - C_t}{M} \times V \quad (5)$$

C_0 and C_t are the initial and final antibiotic concentrations at time t (mg L^{-1}), respectively, V is the volume of wastewater (mL), and M is the mass of the adsorbent (g).[54,58]

3.6. Adsorption study

The prepared GO/PVA/CA composite beads were used to remove CPX from solutions with concentrations of 20, 40, 60, 80, and 100 mg L^{-1}. The effects of the adsorbent dose, concentration, duration, pH, and temperature were observed and discussed accordingly.

3.6.1 Effect of the absorbent dose. The dosage of the adsorbent, which is related to the availability of open active sites, plays a crucial role in the adsorption process. Adsorbents possess a large surface area, providing more binding sites for adsorbing materials.[62]

Therefore, an increase in the mass of the adsorbent in aqueous environments leads to a higher uptake of the adsorbate. Increasing the dosage of adsorbents such as graphene oxide (GO), polyvinyl alcohol (PVA), or calcium alginate (CA) during ciprofloxacin (CPX) adsorption improves overall removal efficiency while decreasing the adsorption capacity per gram of adsorbent. Initially, as the adsorbent dose increases, the removal efficiency increases because more active sites are available to bind to ciprofloxacin molecules. At higher doses of the adsorbent, the adsorption capacity (measured in milligrams of ciprofloxacin adsorbed per gram of the adsorbent) may decrease. This reduction can be attributed to the aggregation of adsorbent particles or saturation, which reduces the effective surface area available for adsorption.[62,63] In this study, varying amounts of the GO/PVA/CA composite beads, ranging from 0.1 to 0.5 g, were used to adsorb ciprofloxacin (CPX). The objective was to evaluate the impact of different dosages of the adsorbent on the removal of ciprofloxacin. The results demonstrating these effects are presented in Fig. 9. As the adsorbent dosage increases from 0.1 to 0.5 g, the percentage of ciprofloxacin removal increases significantly from 19.21% to 75.66%. While increasing the adsorbent dose enhances the overall removal

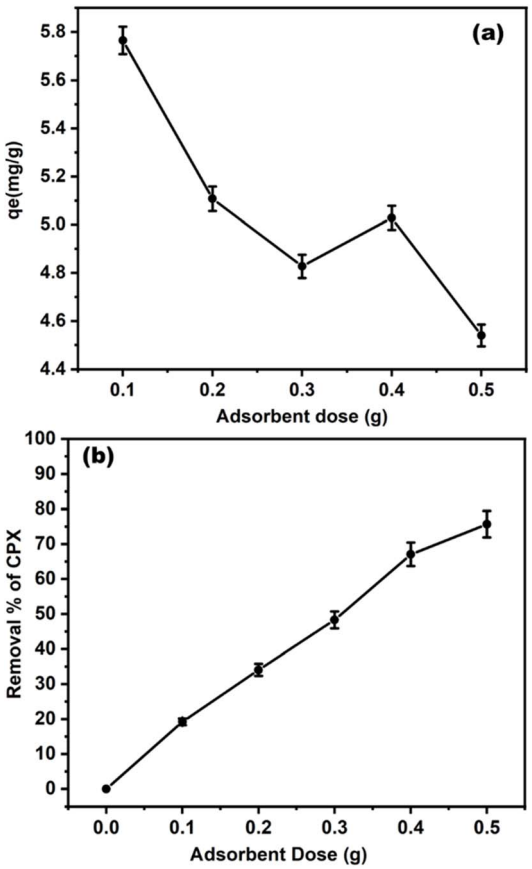

Fig. 9 Influence of adsorbent dose on adsorption capacity (a) and removal efficiency (b).

efficiency up to a certain optimum point, the adsorption capacity per gram tends to decline beyond this threshold due to limitations in available surface sites and the effects of particle aggregation.[54] We determined that the optimal dosage of the GO/PVA/CA adsorbent is 0.5 g, as illustrated in Fig. 9.

3.6.2 Effect of the initial CPX concentration. The adsorption capacity of ciprofloxacin (CPX) on GO/PVA/CA composite beads generally increases with the initial concentration of the adsorbate in the solution. This increase occurs because a higher initial concentration creates a stronger diffusion driving force, allowing more molecules to interact with the active sites of the adsorbent. As the initial concentration of CPX rises, the adsorbent exhibits enhanced adsorption until the active sites are fully saturated. At lower initial CPX concentrations, fewer adsorbate molecules compete for adsorption sites, resulting in a lower adsorption capacity. On the contrary, as the initial concentration of CPX increases, more molecules accumulate on the surfaces of the composite beads, thereby boosting the adsorption capacity. Eventually, the system reaches equilibrium, at which point the maximum site saturation occurs. Beyond this saturation point, further increases in the concentration do not lead to any additional increase in the adsorption capacity. The mechanism has been experimentally validated for similar composites,[63] where an increase in the initial concentration of the adsorbate corresponds to a higher adsorption capacity. This is because of the presence of more adsorbate molecules, which helps overcome the resistance to mass transfer of the active sites on the adsorbent.

Therefore, the initial concentration of CPX directly affects the adsorption capacity of the GO/PVA/CA composite beads by improving the availability and interaction of adsorbate molecules, up to the point of site saturation under batch adsorption conditions.[54] To study the effect of the initial concentration of CPX on the adsorption capacity of the GO/PVA/CA composite beads, 0.5 g of the GO/PVA/CA composite bead sample was added to 50 mL of aqueous solutions with different concentrations of CPX and shaken at 298 K for a contact duration of 150 min. Fig. 10 shows that the adsorption capacity increases as the CPX concentration increases from 20 to 100 mg L^{-1}. The highest CPX adsorption capacity on the GO/PVA/CA composite beads is 7.15 mg g^{-1}, and the removal efficiency first increases and then decreases. The maximum removal efficiency is 89.82% at a concentration of 40 mg L^{-1}.

3.6.3 Effect of the adsorption duration. Analysis of the effect of contact time on the adsorption capacity of ciprofloxacin (CPX) by GO/PVA/CA composite beads indicates that adsorption capacity increases with extended contact time until equilibrium is reached. Initially, many active sites on the

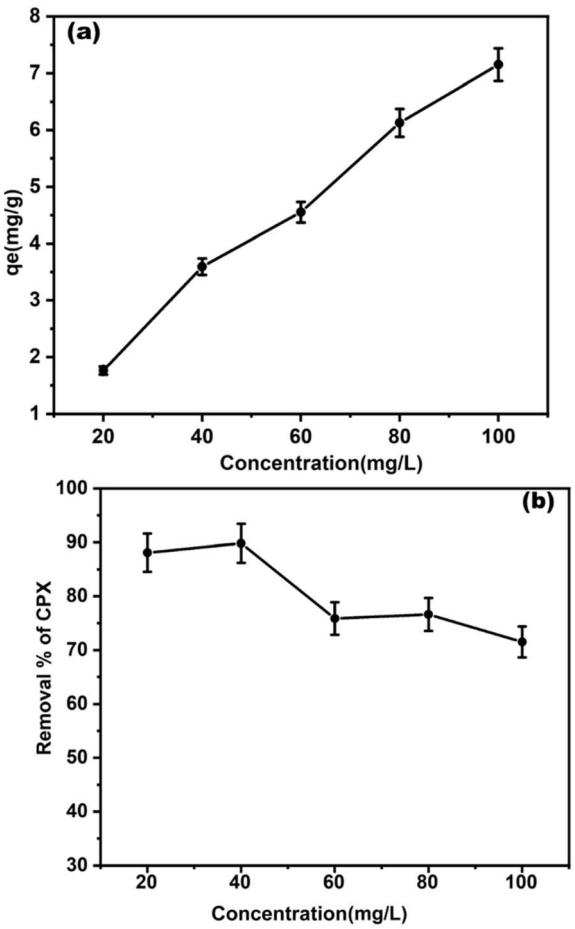

Fig. 10 Effect of the initial concentration on the adsorption capacity (a) and removal efficiency (b).

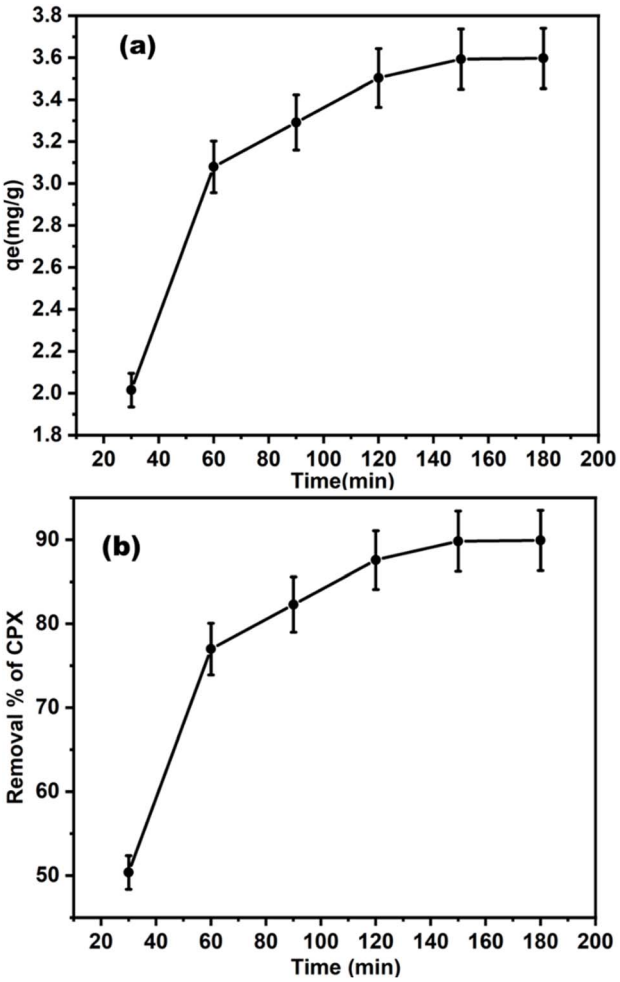

Fig. 11 Effect of contact time on adsorption capacity (a) and removal efficiency (b).

surface of the composite beads are available, allowing rapid adsorption. Over time, as the active sites become saturated, the adsorption rate decreases and ultimately stabilizes at equilibrium. We introduced 0.5 g of the GO/PVA/CA composite bead sample into 50 mL of a 40 mg L^{-1} CPX aqueous solution and agitated it for a specified duration at 298 K. We conducted studies over a period from 30 to 180 minutes at 30-minute intervals to examine the effect of the contact duration on CPX removal. We have presented the percentages of CPX elimination as a function of the contact time in Fig. 11. The adsorption capacity of CPX reaches its peak at a contact time of approximately 150 minutes. After 180 minutes, the adsorption efficiency is around 89.92%, which remains relatively stable from 120 to 180 minutes. This indicates that the optimal time for achieving the adsorption equilibrium of CPX on this composite material is about 150 minutes.

Beyond this timeframe, additional adsorption is minimal, as the active sites available on the adsorbent are saturated.[65] This behavior is typical of adsorption kinetics, where the uptake initially rises rapidly and then stabilizes as equilibrium approaches. The consistent adsorption percentage from 120 to 180 minutes confirms that sufficient active sites are saturated at this point. Therefore, the optimal contact time for the effective removal of CPX is approximately 150 minutes.[64] This is due to the multifunctional properties of the GO/PVA/CA composite bead, which acts as an effective adsorbent, enhancing electrostatic interactions and hydrogen bond formation for exceptional removal efficacy.

3.6.4 Effect of the pH. The adsorption of ciprofloxacin (CPX) from contaminated wastewater is significantly influenced by pH levels. Changes in pH affect adsorption performance by altering both the charge state of ciprofloxacin molecules and the surface charge of the adsorbents.[19,65] Ciprofloxacin is a zwitterionic molecule, which means that it can possess positive and negative charges, depending on the pH. The pK_a value of its carboxylic acid group is approximately 6.1. In contrast, the pK_a value of its amine group ranges from 8.7 to 8.9.[66] Consequently, CPX exists primarily as a cation below pH 6.1, as a zwitterion between pH 6.1 and 8.7, and as an anion above pH 8.7.[67] It is essential to evaluate how the initial pH influences the absorption of CPX. The surface charge of an adsorbent is determined by its point of zero charge (PZC). When the pH is below the PZC, the adsorbent surface is positively charged, whereas above the PZC, it is negatively charged.

The point of zero charge (pHpzc) for the GO/PVA/CA composite is 7.07. At this pH, the material's surface is neutral, as shown in Fig. 5. When the pH of the solution falls below this pHpzc (for example, between pH 4 and 6), the surface of the adsorbent becomes positively charged because of protonation. Conversely, when the pH rises above the pHpzc, the surface becomes negatively charged. Ciprofloxacin (CPX) is an amphoteric molecule with two pK_a values, approximately 6.1 and 8.7. At pH levels between 4 and 6, most CPX molecules exist primarily in their cationic form because the amine group is protonated. In this pH range, the surface of the GO/PVA/CA composite tends to be near or slightly positively charged, which enhances adsorption as a result of attractive electrostatic interactions with the cationic CPX.

Furthermore, other mechanisms, such as hydrogen bonding and π–π interactions, may contribute to increased adsorption. In this pH range, CPX does not convert to its zwitterionic or anionic forms, which would decrease its electrostatic affinity.[68,69]

Therefore, the higher adsorption of CPX at pH 4–6 can be primarily attributed to the electrostatic attraction between the positively charged CPX species and the adsorption surface (as shown in Fig. 12), which is near or slightly below its point of zero charge. This maximizes interactions with functional groups while avoiding the repulsive effects that would occur at pH values above the pHpzc, where the surface becomes more negatively charged, and CPX is likely to exist in zwitterionic or anionic forms. This results in more effective adsorption at a pH slightly below the pHpzc (pH 6 instead of 7.07), as CPX molecules can interact more strongly with the adsorbent without significant electrostatic hindrance.[54]

3.6.5 Effect of the temperature. Temperature plays an important role in determining the adsorption capacity. After adding 0.5 g of the GO/PVA/CA composite bead sample to 50 mL

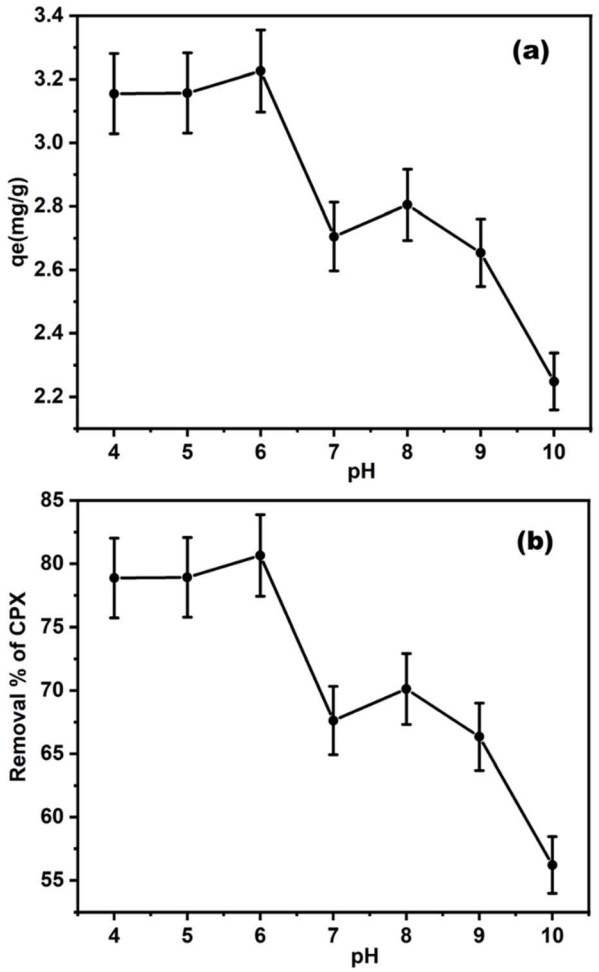

Fig. 12 Effect of the pH on the adsorption capacity (a) and removal efficiency (b).

of an aqueous solution containing 40 mg L^{-1} CPX, the mixture was agitated for 150 minutes.

The test results demonstrate that the GO/PVA/CA composite beads have the best percentage clearance of CPX at 30 °C. The adsorption capacity of ciprofloxacin (CPX) on composite beads made from GO, polyvinylidene, and poly(vinyl alcohol) generally increases with temperature. This suggests that the adsorption process is endothermic and is favored at higher temperatures. The increased temperature likely enhances the mobility of CPX molecules and activates more adsorption sites on the composite beads.[63,70] Conversely, ciprofloxacin adsorption onto GO-based composites decreases as the temperature increases; this indicates an exothermic process. In this case, the temperature increase enhances the solubility of ciprofloxacin in the solution, which reduces its affinity for the adsorbent surface, resulting in a lower amount being adsorbed. This phenomenon is well documented in adsorption studies, where increased solubility counteracts the forces that drive adsorption onto the composite materials.[71]

Typically, the adsorption capacity for ciprofloxacin (CPX) of composite adsorbents such as GO/PVA/CA beads shows a temperature-dependent behavior. The adsorption efficiency increases up to an optimum temperature (around 30 °C in this case, with a removal efficiency of 87.58%) and then gradually decreases beyond this temperature, as shown in Fig. 13. As the temperature increases up to approximately 30 °C, the adsorption capacity improves. This enhancement can be attributed to the increased mobility of the CPX molecules in the solution, which allows greater accessibility to active adsorption sites on the composite. Consequently, this leads to a higher removal efficiency at this optimal temperature. However, beyond the optimal temperature of 30 °C, the adsorption capacity gradually decreases. This decline is often due to the exothermic nature of the adsorption process for such composites. As the temperature increases, the affinity of the adsorbate (CPX) for the adsorbent surface diminishes; this is caused by an increase in the solubility of the drug in the solution and potential changes in the surface porosity or interactions. The decrease in adsorption at higher temperatures suggests that the physical forces responsible for adsorption weaken or that desorption becomes more dominant as the temperature exceeds the optimum.

Therefore, for CPX adsorption on GO/PVA/CA composite beads, there is generally an increase in the adsorption capacity

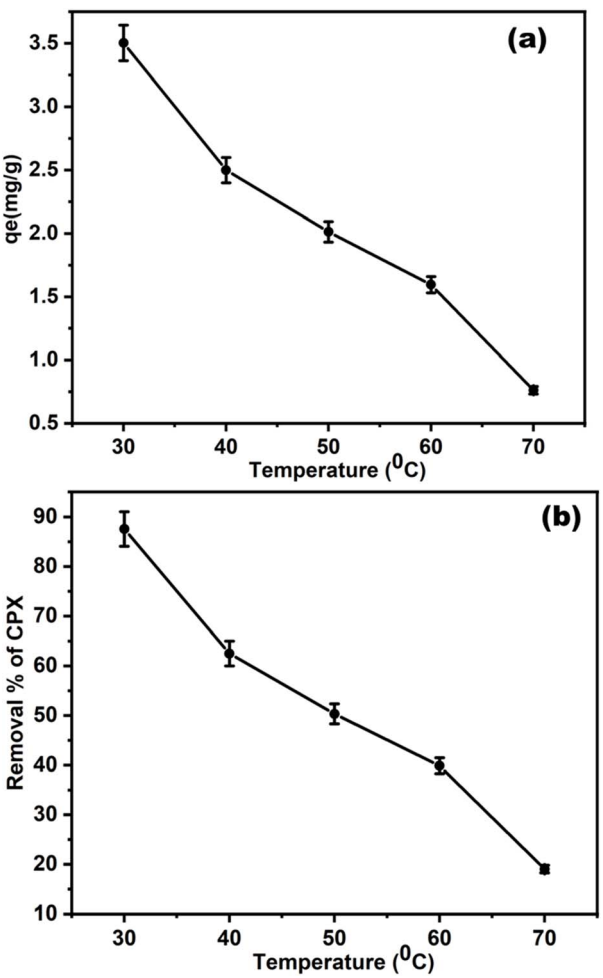

Fig. 13 Effect of the temperature on the adsorption capacity (a) and removal efficiency (b).

with temperature up to a moderate range (around 30 °C). Beyond this point, the capacity may decline as the temperature continues to rise. This behavior reflects a balance between enhanced molecular movement and increased availability of adsorption sites *versus* a reduced affinity for the adsorbent due to increased solubility or structural changes at elevated temperatures.[72]

3.7. X-ray diffraction (XRD) analysis

The XRD analysis confirms the formation of composite beads, highlights the interactions among components, and shows the adsorption of ciprofloxacin (CPX) through peak shifts, appearance or disappearance of peaks, and changes in peak intensity. These changes often indicate alterations in the crystallinity or interlayer spacing. When CPX adsorbs onto the GO/PVA/calcium alginate composite beads, shifts in the characteristic XRD peak positions can occur. This is caused by factors such as lattice strain, intercalation of CPX molecules, or changes in interplanar spacing as a result of interactions among the components. Generally, a shift in peaks toward lower 2θ angles indicates lattice expansion, while a shift toward higher 2θ angles indicates lattice contraction. Moreover, the intensity of the peaks often decreases after CPX adsorption. This reduction can be attributed to an increased lattice disorder, a decreased crystallite size, or the formation of an amorphous phase resulting from the incorporation of the drug. Additionally, the broadening of the XRD peaks after adsorption is common and is related to the introduction of microstrain or defects. In composites such as GO/PVA/calcium alginate, the distinctive (001) peak of GO, which appears near 14.9°, loses intensity, indicating changes in interlayer spacing due to CPX adsorption. Before adsorption, the most prominent peak for GO occurs at $2\theta = 28.26°$. At this angle, the *d*-spacing measures 3.156, and the *hkl* crystal structure corresponds to the d_{031} plane. This angle decreases after adsorption, and the value of the *d*-spacing and crystal structure are 1.23 and d_{222}, respectively. The peak intensities of PVA may also decrease or broaden as a result of interactions between the polymer chains and CPX. Calcium alginate generally contributes broad amorphous patterns, which may also exhibit slight changes. The disappearance or reduction of crystalline peaks associated with CPX in the XRD pattern after adsorption suggests that CPX may convert into an amorphous or molecularly dispersed state within the composite matrix. Quantitative peak analysis often focuses on changes in the peak position, intensity, and FWHM to infer the effects of adsorption on crystallinity and lattice parameters. The XRD peaks observed for the GO/PVA/calcium alginate composite beads before the adsorption of ciprofloxacin (CPX) at 14.920°, 28.26°, and 32° likely correspond to the characteristic crystalline or semicrystalline structures of the composite materials. After CPX adsorption, the sharp peaks at 27.86°, 44°, 64.4° and 77.5° indicate a change in the crystallinity or the appearance of new crystalline phases due to the interaction or binding of ciprofloxacin on the beads, as shown in Fig. 14.

The observed shift in the XRD peaks indicates that the adsorption of CPX alters the structural properties of the composite beads. This alteration may be due to physical adsorption or chemisorption interactions that modify lattice spacings or create new ordered domains within the adsorbent matrix. Changes in peak positions and intensities after adsorption are typical, as they reflect the successful binding of the adsorbate and potential rearrangement or cross-linking within the polymer matrix. Additionally, the presence of new characteristic peaks or shifts in FTIR and XRD spectra after adsorption highlights the physical adsorption mechanisms and effective interactions between the adsorbent and the adsorbate.[73] Therefore, changes in the XRD patterns before and after CPX adsorption confirm that the GO/PVA/calcium alginate composite beads undergo structural modifications as a result of CPX binding, as evidenced by the appearance of new and shifted crystalline peaks.

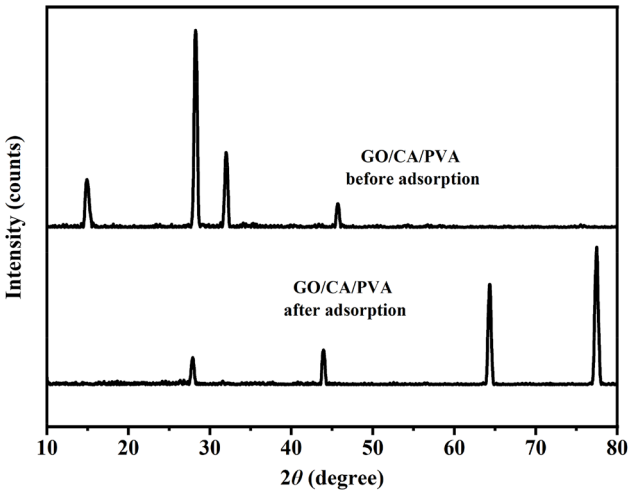

Fig. 14 XRD analysis of the GO/PVA/CA composite beads before and after adsorption.

3.8. SEM studies

Studies have reported the SEM images of composite beads made from combinations of graphene oxide (GO), polyvinyl alcohol (PVA), and calcium alginate.[54,74]

These beads are typically prepared by mixing sodium alginate and PVA in a dispersion of GO, followed by crosslinking with calcium ions. Numerous polygonal pores with thin walls and open pores are visible for the 5% PVA, 5% SA, and 1% GO composite bead hydrogel. The SEM images generally illustrate the morphology and surface texture of the resulting composite beads, as shown in Fig. 15(a). They usually exhibit a spherical shape and a carbonaceous structure due to the presence of GO, PVA, and calcium alginate. The surface morphology, characterized by increased porosity and roughness due to the incorporation of GO, leads to a larger surface area for adsorption.

Images may reveal some irregularities, such as cracks and pores. The size and distribution of these pores are influenced by the composition and cross-linking method. Compared to pure alginate beads, the rougher surface morphology suggests enhanced mechanical stability and more active adsorption

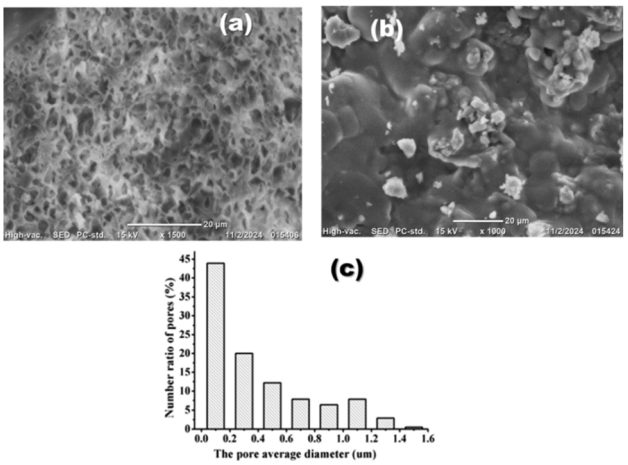

Fig. 15 SEM images (a) before adsorption and (b) after adsorption. (c) Average pore diameter.

sites, attributable to the polymer blend (comprising PVA and alginate) and the presence of GO. Fig. 15(b) shows the scanning electron microscopy (SEM) image of the GO/PVA/CA composite bead surface after ciprofloxacin adsorption. The surface becomes relatively smoother, and many pores are blocked or covered by adsorbed molecules. This morphological change confirms that adsorption occurs because the porous network is less visible compared to the pristine sample. The pore size distribution in Fig. 15(c) indicates that before adsorption, most of the pores are concentrated within the 0.1–0.4 μm diameter range, with the highest frequency (~43%) at approximately 0.2 μm. This indicates that the GO/PVA/CA composite beads possess a micro–mesoporous network. Such small pore diameters are advantageous because they increase the surface area and improve the accessibility of the adsorption sites, facilitating the diffusion and binding of ciprofloxacin molecules. The presence of a few larger pores (>1.0 μm) suggests heterogeneity in the pore structure, which may further aid in mass transport during adsorption. The pore size distributions of the GO/PVA/CA composite beads were examined using Image-Pro Plus software before and after adsorption.

The dispersion of GO within the PVA/alginate matrix is typically uniform, resulting in a composite with good mechanical and adsorption properties.[54,74] These characteristics collectively enhance adsorption performance by providing ample interaction sites and favorable diffusion channels for target molecules.

3.9. Energy-dispersive X-ray spectroscopic (EDS) analysis

The energy-dispersive X-ray spectroscopic (EDS) analysis of composite beads made from graphene oxide (GO), polyvinyl alcohol (PVA), and calcium alginate, both before and after ciprofloxacin (CPX) adsorption, reveals significant changes in the elemental composition, which indicates successful adsorption.

Before the adsorption process, the EDS spectrum typically shows elements corresponding to the constituents of the beads: carbon from GO and PVA, oxygen from alginate and GO, calcium from calcium alginate, and possibly other trace elements depending on the synthesis method.[75] After CPX adsorption, the EDS spectrum displays new or intensified signals for elements associated with the CPX molecule, particularly nitrogen from the amine groups and fluorine, which is distinctive to CPX. The increase in the intensity of the nitrogen peak confirms the adsorption of CPX molecules onto the composite surface. Furthermore, the relative atomic percentages of carbon and oxygen may change as a result of surface coverage by CPX. The calcium signal may also vary depending on its interaction with CPX. These changes in EDS observed before and after adsorption provide elemental evidence supporting the capture of CPX by the composite beads. This finding complements other characterization techniques, such as FTIR spectroscopy. The elemental composition of the GO/PVA/CA composite beads before and after adsorption was analysed using EDS, as shown in Fig. 16 and 17.

The energy-dispersive X-ray spectroscopic (EDS) analysis of the GO/PVA/CA composite beads both after and before ciprofloxacin adsorption indicates significant changes in the elemental composition, confirming successful adsorption and interaction. The elemental composition changes, as indicated by an increase in the mass percentage of carbon (C) from 19.27% before treatment to 29.60% after treatment. This indicates the addition of ciprofloxacin, an organic compound, to the surface of the beads. The oxygen (O) mass% decreases from

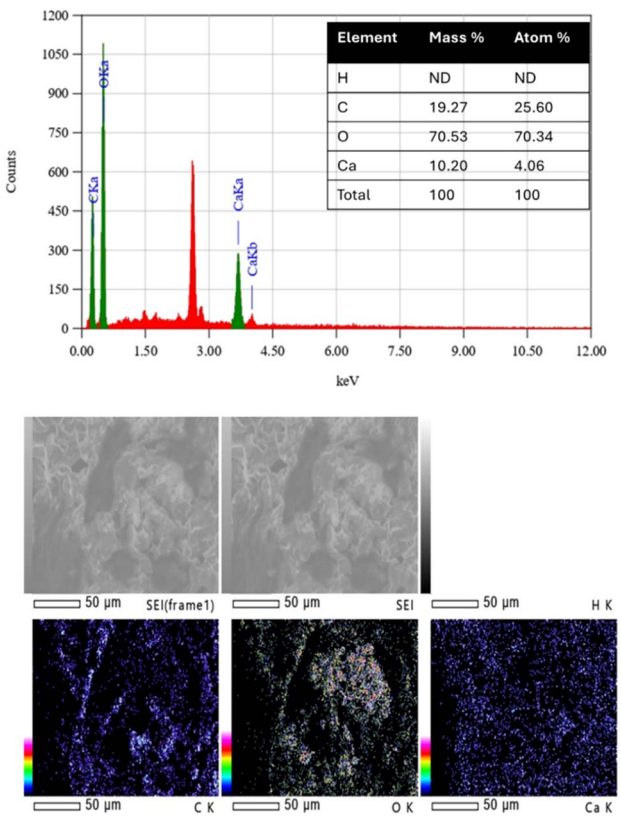

Fig. 16 EDS analysis of the GO/PVA/CA composite beads before adsorption.

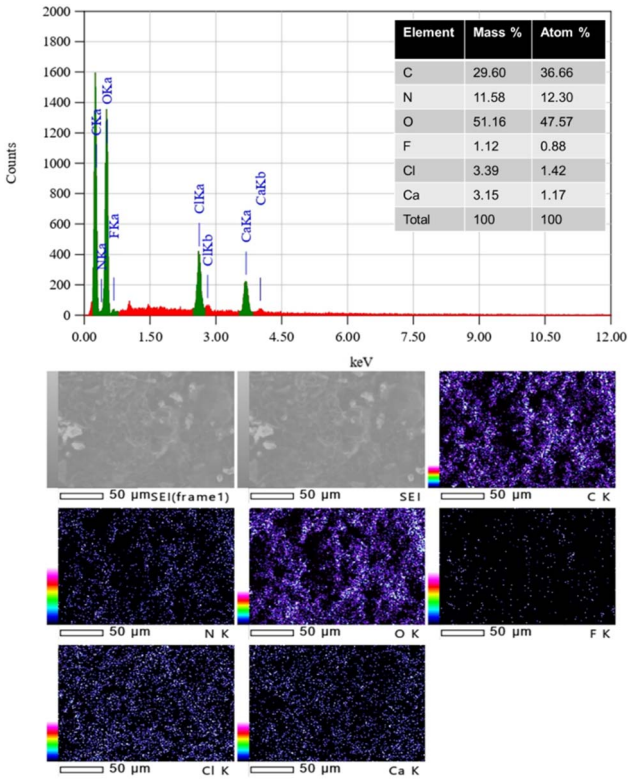

Fig. 17 EDS analysis of the GO/PVA/CA composite beads after adsorption.

70.53% (before) to 51.16% (after). This suggests that CPX occupies oxygen-rich groups (*e.g.*, carboxyl and hydroxyl) on the surface, reducing detectable oxygen. The mass percentage of calcium (Ca) decreased from 10.20% before treatment to 3.15% after treatment. This reflects the role of calcium in interactions with CPX, possibly through ionic bonding or partial surface coverage. Nitrogen (N) is present at a mass percentage of 11.58% in the post-adsorption spectrum, while it is not detected in the pre-adsorption spectrum. This confirms the presence of ciprofloxacin, which contains nitrogen in its molecular structure. The post-adsorption spectrum indicates that fluorine (F) is present at 1.12% by mass. This is a unique marker of CPX that confirms its adsorption onto the composite beads. Chlorine (Cl) is present at a mass percentage of 3.39% in the post-adsorption spectrum. The product probably originates from CPX or residual chemicals in wastewater.

Carbon and oxygen molecules are uniformly distributed across the bead surface before adsorption. Following adsorption, an increase in carbon content and a decrease in oxygen content are observed, which suggests surface interaction with CPX molecules. Nitrogen and fluorine are not present before adsorption but are clearly visible after adsorption, confirming the adsorption of CPX onto the composite beads. Calcium's intensity decreases after adsorption, suggesting its role in CPX binding or interaction.

The EDS analysis also highlights the probable mechanism: (a) hydrogen bonding: CPX with oxygen-rich functional groups (carboxyl, hydroxyl) of the composite beads. (b) Electrostatic interactions: potential interaction between CPX's negatively charged functional groups and calcium ions. (c) π–π interactions: the carbonaceous structure of graphene oxide may also make adsorption easier by forming π–π stacking with the aromatic rings of CPX.

3.10. Adsorption isotherm

Adsorption isotherms provide crucial theoretical parameters for the design and development of simulated adsorption systems by describing the interaction between the adsorbent and the adsorbate at a fixed pH and temperature. By adjusting the CPX concentration between 20 and 100 mg L^{-1}, the adsorption isotherm was investigated. 0.5 g of GO/PVA/CA composite beads was added to 50 mL of CPX (concentration = 40 mg L^{-1}) using the batch adsorption technique. The mixture was agitated at 200 rpm, while the absorption of CPX on the composite beads was tracked at different intervals between 30 and 180 minutes. In this work, the equilibrium CPX adsorption data of the GO/PVA/CA composite beads were analysed using the linear and nonlinear Langmuir, Freundlich, Temkin, and Dubinin–Radushkevich (D–R) isotherm models, as shown in Fig. 18 and 19. Table 2 presents the parameters of the linear adsorption isotherm models, and those of the nonlinear adsorption models are summarized in Table 3.

Four different isotherm models, namely, Langmuir, Freundlich, Temkin, and Dubinin–Radushkevich (D–R), were used in their linear and nonlinear forms to investigate the type of adsorption process, either monolayer or multilayer.[49,76,77]

Adsorption isotherms describe how adsorbents interact with adsorbent materials, and the Langmuir (monolayer),[78] Freundlich (multilayer/heterogeneous), Temkin (heat of adsorption), and D–R (porous filling) models are critical. Nonlinear models directly fit experimental data to avoid distortion of errors, while linear models are used for graphical parameter determination. The Langmuir linear and nonlinear isotherms' mathematical forms are as follows:

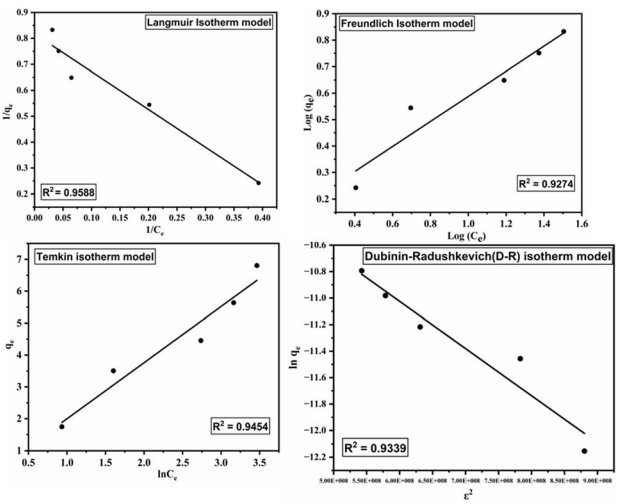

Fig. 18 Linear fits of Langmuir, Freundlich, Temkin, and Dubinin–Radushkevich (D–R) adsorption isotherm models.

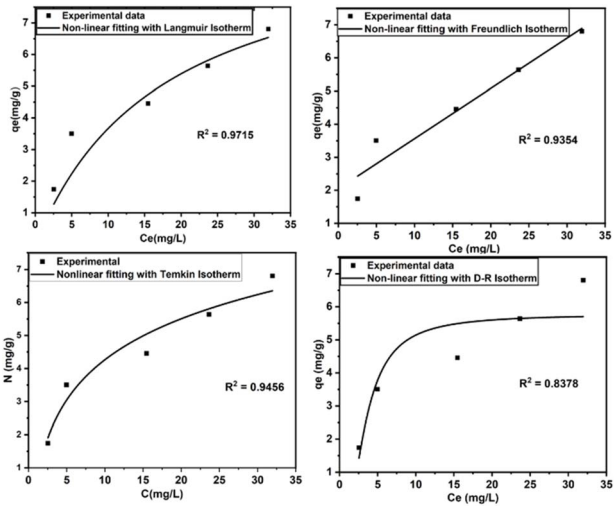

Fig. 19 Nonlinear fits of the Langmuir, Freundlich, Temkin, and Dubinin–Radushkevich (D–R) adsorption isotherm models.

$$\frac{1}{q_e} = \frac{1}{q_m} + \frac{1}{q_0 b C_e} \tag{6}$$

$$q_e = \frac{q_m k_L C_e}{1 + k_L C_e} \tag{7}$$

Here, C_e is the equilibrium concentration of the adsorbate (mg L^{-1}); q_e is the adsorption capacity at equilibrium (mg g^{-1}); q_m is the maximum capacity (mg g^{-1}); and b (L mg^{-1}) is the Langmuir constant. From the Langmuir equation, the slope and intercept of the plot of $1/C_e$ *versus* $1/q_e$ are used for the calculation of b and q_m, respectively.

The Freundlich adsorption isotherms' linear and nonlinear mathematical forms are as follows:

$$\ln q_e = \ln K_F + \frac{1}{n} \ln C_e \tag{8}$$

$$q_e = K_F C_e^{\frac{1}{n}} \tag{9}$$

Here, K_F (mg g^{-1}) is the adsorption capacity, and n is the intensity.

The Temkin adsorption isotherms' linear and nonlinear mathematical forms are as follows:

$$q_e = \frac{RT}{b_T} \ln A_T \left(\frac{RT}{b_T}\right) \ln C_e \tag{10}$$

$$q_e = \frac{RT}{b_T} \ln(A_T C_e) \tag{11}$$

Here, A_T (L mg^{-1}) is the equilibrium binding constant, and b_T (J mol^{-1}) is related to heat sorption.

The Dubinin–Radushkevich (D–R) adsorption isotherms' linear and nonlinear mathematical forms are as follows:

$$\ln q_e = \ln q_s - K_{ad}\varepsilon^2 \tag{12}$$

$$q_e = q_s \exp(-K_{ad}\varepsilon^2) \tag{13}$$

Here, q_s is the saturation capacity, K_{ad} is a constant related to the mean adsorption energy, and ε is the Polanyi potential, $\varepsilon = RT \ln\left(1 + \frac{1}{C_e}\right)$.

The Freundlich ($R^2 = 0.9274$), Langmuir ($R^2 = 0.9588$), Temkin ($R^2 = 0.9454$), and Dubinin–Radushkevich (D–R) ($R^2 = 0.9339$) models at 40 °C are well-fitted, as indicated by their R^2 values. The adsorption of CPX on GO/PVA/CA is a multilayer process on heterogeneous surfaces, as indicated by the Freundlich adsorption isotherms. By contrast, the electrostatic interaction involved in the adsorption process is demonstrated by a suitable fitting of the Temkin model.

Nonlinear adsorption isotherm models fit CPX adsorption equilibrium data onto graphene oxide/polyvinyl alcohol/calcium alginate (GO/PVA/CA) composites with greater accuracy than linear models, thereby minimizing transformation biases. The results indicate that the nonlinear Langmuir isotherm model exhibits the highest correlation with the experimental data ($R^2 = 0.9715$). This model characterizes adsorption as the formation of a single layer of adsorbate molecules on a surface with uniform adsorption sites, each possessing identical energy. Consequently, each active site binds only one CPX molecule, and no further adsorption occurs at occupied sites. The high maximum monolayer adsorption capacity of 10.14 mg g^{-1} demonstrates a strong affinity between the composite material and CPX.

The Freundlich isotherm's n parameter, being greater than 1, indicates that the adsorption process is favorable. The Temkin model suggests the presence of moderate energy interactions

Table 2 Parameters of linear adsorption isotherm models[79]

Linear fit of the Langmuir isotherm model	q_m (mg g^{-1})	8.210
	R^2	0.9588
	K_L (L mg^{-1})	0.30 to 0.08
Linear fit of the Freundlich isotherm model	K_F (mg g^{-1})	1.1207
	R^2	0.9274
	n	2.11059
Linear fit of the Temkin isotherm model	B_T (J mol^{-1})	1429.26
	R^2	0.9454
	A_T (L mg^{-1})	1.120763
Linear fit of the Dubinin–Radushkevich (D–R) model	q_m (mg g^{-1})	0.00013811
	R^2	0.9339
	E (kJ mol^{-1})	11 800

Table 3 Parameters of nonlinear adsorption isotherm models

Nonlinear fit of the Langmuir isotherm model	q_m (mg g^{-1})	10.14
	R^2	0.9715
	K_L (L mg^{-1})	0.0566
Nonlinear fit of the Freundlich isotherm model	K_F (mg g^{-1})	2.0439
	R^2	0.9354
	n	6.5888
Nonlinear fit of the Temkin isotherm model	B_T (J mol^{-1})	1.829
	R^2	0.9456
	A_T (L g^{-1})	0.2974
Nonlinear fit of the Dubinin–Radushkevich (D–R) model	q_m (mg g^{-1})	5.7715
	R^2	0.8378
	E (kJ mol^{-1})	0.1984

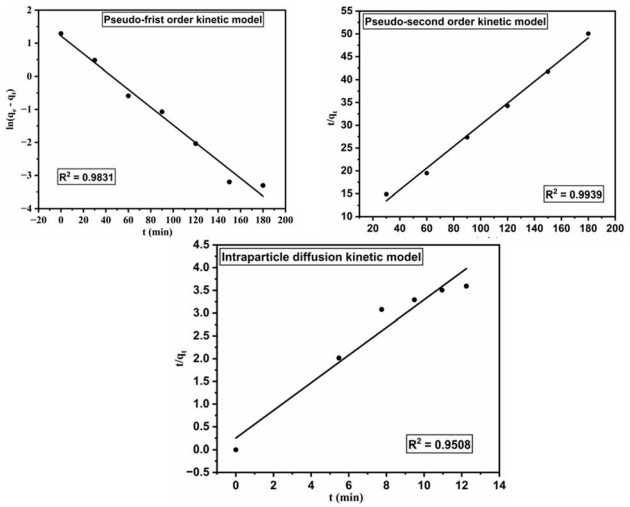

Fig. 20 Linear pseudo-first-order kinetic model, pseudo-second-order kinetic model, and intraparticle diffusion kinetic model of the GO/PVA/CA composite beads.

between CPX and the adsorbent. However, the superior fit of the nonlinear Langmuir model, which directly represents the experimental data without mathematical transformations, validates the concept of monolayer adsorption, as shown in Fig. 19. To further elucidate the CPX adsorption mechanism on the GO/PVA/CA composite, the Dubinin–Radushkevich (D–R) isotherm model was applied. The linear relationship observed in the plot of ln q_e against ε^2 (the Polanyi potential), as shown in Fig. 18, with a high coefficient of determination ($R^2 = 0.9339$ for the linear model and 0.8378 for the nonlinear model), supports the applicability of this model. The D–R constant (β) is determined, and the mean free energy of adsorption (E) is calculated to be 0.1984 kJ mol^{-1} in the nonlinear fitting. The findings from the D–R model are consistent with those from the Langmuir and Freundlich models. These results further support the conclusion that adsorption occurs on a largely uniform surface, as indicated by the Langmuir model, through a physical mechanism. This is consistent with the low energy requirement and the observed reversible nature of the adsorption process in the regeneration study.

3.11. Adsorption kinetic study

Adsorption kinetics is the study of the physical and/or chemical interactions between adsorbent and adsorbate species. 50 mL of CPX (concentration = 40 mg L^{-1}) was mixed with 0.5 g of the GO/PVA/CA composite beads for kinetic modelling. The

Table 4 Summary of the kinetic parameters for linear and nonlinear pseudo-first-order, pseudo-second-order, and intraparticle diffusion models

Linear pseudo-first-order kinetic model	q_e (mg g^{-1})	3.3753
	R^2	0.9831
	k_1 (min^{-1})	−0.00018
Linear pseudo-second-order kinetic model	q_e (mg g^{-1})	4.38058
	R^2	0.9939
	k_2 (g mg^{-1} min^{-1})	0.007446
Linear intraparticle diffusion	k_{id} (mg g^{-1} min$^{-1/2}$)	0.304
	R^2	0.9508
	C (mg g^{-1})	0.251
Nonlinear pseudo-first-order kinetic model	q_e (mg g^{-1})	3.3675
	R^2	0.9979
	k_1 (min^{-1})	0.028 ± 0.001
Nonlinear pseudo-second-order kinetic model	q_e (mg g^{-1})	4.45827
	R^2	0.9941
	k_2 (g mg^{-1} min^{-1})	0.0069
Nonlinear intraparticle diffusion	k_{id} (mg g^{-1} min$^{-1/2}$)	1.0366
	R^2	0.9767
	C (mg g^{-1})	9.99 × 10^{-26}

adsorption of CPX on the GO/PVA/CA composite beads was carried out at different intervals between 30 and 180 minutes. The mixture solution was maintained at 200 rpm simultaneously. To analyze the kinetics data, we took into account the Weber–Morris intraparticle diffusion, Ho's pseudo-second-order, and Lagergren's pseudo-first-order models. The integral forms of the pseudo-first-order, pseudo-second-order, and Weber–Morris intraparticle diffusion models are expressed by the following equations:[80]

$$\ln(q_t - q_e) = \ln q_e + k_1 t \quad (14)$$

$$q_t = q_e(1 - e^{-k_1 t}) \quad (15)$$

where q_t is the adsorption capacity at time t (mg g^{-1}), q_e is the equilibrium capacity (mg g^{-1}), and k_1 is the rate constant.

Pseudo-second-order model:

$$\frac{t}{q_t} = \frac{1}{k_2 q_e^2} + \frac{t}{q_e} \quad (16)$$

$$\frac{d_{q_t}}{dt} = k_2(q_e - q_t)^2 \quad (17)$$

q_t is the adsorption capacity at time t, q_e is the equilibrium capacity (mg g^{-1}), and k_2 is the rate constant (g mg^{-1} min^{-1} or L mmol^{-1} min^{-1}).

Intraparticle diffusion model:

$$q_t = k_{id} t^{1/2} + C \quad (18)$$

where q_t is the amount adsorbed at time t (mg g^{-1}), k_{id} is the intraparticle diffusion rate constant (mg g^{-1} min$^{-1/2}$), $t^{1/2}$ is the square root of the contact time (min), and C is the intercept reflecting boundary layer effects (mg g^{-1}).

The linearized form of the model equation, depicted in Fig. 20, was used to analyze the experimental data. Table 3 displays the different kinetic characteristics associated with CPX adsorption on the GO/PVA/CA composite beads. For intraparticle diffusion, pseudo-first-order, and pseudo-second-order models, the correlation coefficients (R^2) are 0.9831, 0.9939, and 0.9508, respectively.

Nonlinear pseudo-first-order, pseudo-second-order, and intraparticle diffusion models describe the adsorption kinetics of ciprofloxacin (CPX) onto graphene oxide (GO)/PVA/calcium alginate beads, revealing chemisorption and diffusion mechanisms.

These models fit experimental data from similar GO/calcium alginate systems, where CPX adsorption reaches capacities around 6.8 mg g^{-1}, though PVA addition enhances bead stability and surface functionality for better uptake, as reported in the literature.[54]

The pseudo-second-order (PSO) model often yields the highest R^2 (>0.99) and q_e matching experiments, outperforming the pseudo-first-order (PFO) model (lower q_e, $R^2 \approx 0.99$) and confirming rate-limiting chemisorption. Intraparticle diffusion (IPD) plots exhibit two distinct linear stages: an initial rapid external diffusion phase (k_{id}, high), followed by a slower intraparticle diffusion phase (k_{id} lower, $C > 0$). These results indicate

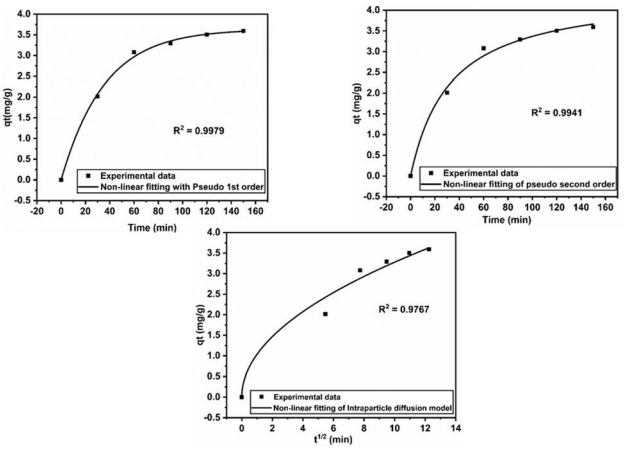

Fig. 21 Nonlinear pseudo-first-order kinetic model, pseudo-second-order kinetic model, and intraparticle diffusion kinetic model of the GO/PVA/CA composite beads.

Table 5 Thermodynamic parameters for the adsorption of CPX onto GO/PVA/CA

Temperature (K)	$\Delta G°$ (kJ mol^{-1})	$\Delta H°$ (kJ mol^{-1})	$\Delta S°$ (J mol^{-1} K^{-1})	R^2
303	−13.74	−66.9	−177.4	0.9581
313	−10.44			
323	−9.434			
333	−8.855			
343	−5.857			

that while diffusion contributes to adsorption, it does not solely govern the process, as shown in Fig. 21 and Table 4. Surface interactions between the functional groups of graphene oxide (GO) and the ion-exchange properties of alginate also play significant roles.

For CPX adsorption on GO/alginate beads, PVA crosslinks improve porosity, boosting the PSO fit and IPD multistages,

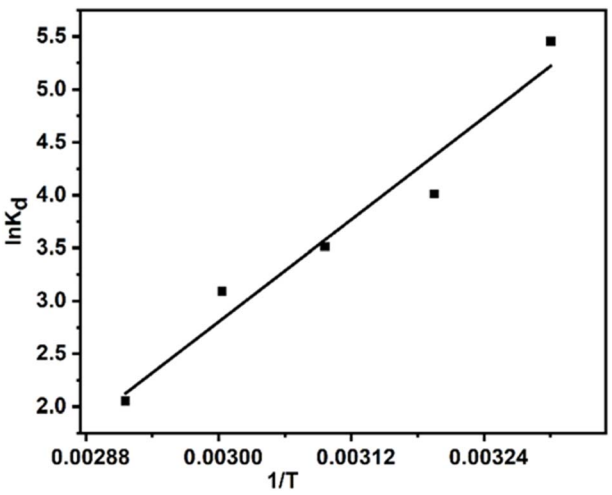

Fig. 22 Thermodynamic analysis plot for CPX adsorption on GO/PVA/CA.

Table 6 Comparison study of the present work with other reported articles

Adsorbent	Max. capacity (mg g^{-1})	Key driving factors
GO/CA fibers (6% GO)[22]	39.06	High porosity, GO sheets
GO/Ca-Alg–PAM beads[54]	6.85	Dense double-network
GO/PVA/alginate DN hydrogel[85]	Improved *vs.* control	Larger pores, functional groups
GO/PVA/calcium alginate (Present work)	10.14	Structure, functional groups

with exothermic/spontaneous thermodynamics (negative $\Delta G°$ and $\Delta H°$) favoring low-temperature operations.

All three kinetic models closely match the kinetic data, as shown by the R^2 values. The adsorption process satisfies the pseudo-second order kinetics model. These findings indicate that the rate-determining process is most likely chemisorption, which involves the sharing or exchange of electrons between the adsorbent and adsorbate through valence forces.

3.12. Thermodynamic analysis

The thermodynamic analysis of ciprofloxacin (CPX) adsorption onto the GO/PVA/calcium alginate composite often involves calculating several parameters, such as Gibbs free energy change (ΔG), enthalpy change (ΔH), and entropy change (ΔS). A negative ΔG ($-\Delta G$) in adsorption thermodynamics means that the process is spontaneous. Negative ΔG values indicate that adsorption occurs naturally without the need for additional energy input, which is a favorable characteristic for adsorption.[81]

Typically, ΔG is calculated using the equation:

$$\Delta G = -RT \ln K_c \tag{19}$$

$\ln K_c = R\Delta S - RT\Delta H$ is used to derive ΔH and ΔS from a van't Hoff plot.

$$\ln K_c = \frac{\Delta S}{R} - \frac{\Delta H}{RT} \tag{20}$$

where R is the gas constant, T is the temperature in Kelvin, and K_c is the equilibrium constant for adsorption. The negative sign before ΔG signifies the spontaneous nature when the logarithm of K_c is positive.

In adsorption thermodynamics, negative values of Gibbs free energy change (ΔG), enthalpy change (ΔH) and entropy change (ΔS) provide important insights into the adsorption process: a negative ΔG indicates that the adsorption process is spontaneous and thermodynamically favorable at the given temperature, as shown in Table 5 and Fig. 22. A negative ΔH signifies that the process is exothermic, which means that it releases heat during adsorption, and a negative ΔS suggests a decrease in randomness or disorder at the solid–adsorbate interface, indicating that molecules become more ordered when adsorbed.[82]

Therefore, when ΔG, ΔH, and ΔS are all negative, the adsorption is spontaneous and exothermic, with the adsorbate molecules becoming more structured on the adsorbent surface. This ordered arrangement results in entropy loss; however, the exothermic nature and spontaneity propel the process forward.[83]

3.13. Cost analysis

GO/PVA/calcium alginate composites are promising, cost-effective adsorbents for ciprofloxacin removal from wastewater owing to their biocompatibility, the high surface area provided by graphene oxide (GO), and the bead-forming capability of calcium alginate crosslinked with polyvinyl alcohol (PVA), which facilitates easy separation (Table 6).

The synthesis process utilizes low-cost materials, including GO (approximately $50–200 per kilogram industrially), PVA ($2–5 per kilogram), sodium alginate ($5–10 per kilogram), and the $CaCl_2$ cross-linker ($1 per kilogram). The total material cost per kilogram of beads is estimated to be $10–30. This process is scalable through simple drop-wise extrusion into a $CaCl_2$ bath and does not require high-energy steps. This composite excels in cost-effectiveness for large-scale environmental applications like pharmaceutical wastewater treatment.[84]

Desorption uses mild acid/alkali (*e.g.*, 0.1 M HCl or NaOH, <$0.5 per L), enabling 4–5 cycles with <25% capacity loss. The operational cost per cycle is $0.1–0.5 per kg wastewater treated (0.1 g beads per L), assuming a 100 L batch; the total lifecycle cost is <$1 per kg of CPX removed over 5 cycles. This composite excels in cost-effectiveness for large-scale environmental applications like pharmaceutical wastewater (CPX) treatment.[63]

4. Conclusion

This study successfully developed and characterized GO/PVA/CA composite beads, demonstrating their suitability as an advanced adsorbent for the effective removal of CPX from contaminated aqueous solutions. Composite beads achieved a maximum removal efficiency of 89.82% under optimal conditions, demonstrating their effectiveness in the elimination of pharmaceutical contaminants. The composite beads also demonstrated high reusability, with an efficiency of more than 85% after five adsorption–desorption cycles. The adsorption isotherm model and kinetic model were favorable for this adsorbent. Among the analysis of isotherm models, the Langmuir model suggests monolayer adsorption, while the Freundlich model indicates slightly heterogeneous binding. The kinetic studies suggest that the reaction follows a pseudo-second-order model, indicating strong chemical interactions. The adsorption process was driven primarily by π–π interactions, hydrogen bonding, and (slightly) electrostatic forces. The ΔG, ΔH, and ΔS values were negative, which implied that the

adsorption was spontaneous and exothermic. The ecofriendly and biodegradable nature of the composite materials, coupled with their high adsorption efficiency, underscores their potential as a sustainable solution for wastewater treatment, aligning with global efforts to combat water pollution. This work lays the foundation for further exploration into the scalability of these composite beads in real-world wastewater systems, multi-contaminant removal studies, and reusability optimization for enhanced cost efficiency.

Author contributions

The manuscript was written through the contributions of all authors. All authors have approved the final version of the manuscript. The authors, Md. Samrat Hossain and Md. Anwarul Karim, have equal contributions in this work.

Conflicts of interest

The authors declare no conflict of interest.

Data availability

All data generated in this study are included in the manuscript.

Acknowledgements

This research was supported by the regular program of education of the Department of Applied Chemistry and Chemical Engineering, Faculty of Engineering, University of Rajshahi, Bangladesh.

References

1 F. Li, J. Huang, M. Wang, L. Chen and Y. Xiao, *Aquaculture*, 2021, **545**, 737200.
2 D. Zheng, G. Yin, M. Liu, C. Chen, Y. Jiang, L. Hou and Y. Zheng, *Sci. Total Environ.*, 2021, **777**, 146009.
3 Z. Yang, X. Li and K. Yan, *J. Cleaner Prod.*, 2021, **310**, 127584.
4 S. Youcef, M. Chebbi, L. Youcef, M. G. Bouaziz, A. Soudani, A. Sahli and C. Deroues, *Environ. Monit. Assess.*, 2025, **197**, 536.
5 M. Chebbi, S. Youcef, L. Youcef, A. Soudani, C. Dridi, A. Sahli, A. Houchete and C. Deroues, *RSC Adv.*, 2024, **14**, 37833–37845.
6 M. A. Karim, M. R. Rahman, S. S. Dipti and M. M. E. Elahi, *J. Water Environ. Technol.*, 2024, **22**(1), 41–52.
7 F. Sordello, D. Fabbri, L. Rapa, C. Minero, M. Minella and D. Vione, *J. Cleaner Prod.*, 2021, **289**, 125722.
8 S. Youcef, L. Youcef, O. Kheliel, M. A. Khelfa, F. N. Chergui, R. Kara, S. Ziad, M. Chebbi, M. Benakcha, S. Guergazi and C. Dridi, *React. Kinet., Mech. Catal.*, 2025, **97**, 536.
9 A. Soudani, L. Youcef, S. Youcef, S. Elbahi, K. Toumi, G. Saadia, A. Sahli and N. Soudani, *Chem. Afr.*, 2024, **7**, 3903–3915.
10 S. Youcef, L. Youcef, O. Kheliel, M. A. Khelfa, F. N. Chergui, R. Kara, S. Ziad, M. Chebbi, M. Benakcha, S. Guergazi and C. Dridi, *React. Kinet., Mech. Catal.*, 2026, DOI: 10.1007/s11144-026-03035-x.
11 S. Youcef, S. Guergazi and L. Youcef, *Model. Earth Syst. Environ.*, 2022, **8**, 3927–3940.
12 A. Soudani, L. Youcef, L. Bulgariu, S. Youcef, K. Toumi and N. Soudani, *Chem. Eng. Res. Des.*, 2022, **188**, 972–987.
13 L. Zhao, Y. Ji, J. Yao, S. Long, D. Li and Y. Yang, *J. Cleaner Prod.*, 2017, **2168**, 626–631.
14 F. He, W. Cai, J. Lin, B. Yu, G. Owens and Z. Chen, *J. Cleaner Prod.*, 2021, **293**, 126207.
15 Q. Zhang, D. Fan, X. Pang, W. Zhu, J. Zhao and J. Xu, *J. Cleaner Prod.*, 2021, **292**, 125909.
16 D. Lu, S. Xu and J. Ma, *J. Cleaner Prod.*, 2020, **264**, 121644.
17 G. Zhang, Z. Zhao and Y. Zhu, *J. Cleaner Prod.*, 2020, **256**, 120314.
18 F. Yu, S. Sun, S. Han, J. Zheng and J. Ma, *Chem. Eng. J.*, 2016, **285**, 588–595.
19 C. T. Umeh, J. K. Nduka, K. G. Akpomie, J. O. Ighalo and R. Mogale, *ACS Omega*, 2025, **10**(4), 3784–3800.
20 R. Gothwal and T. Shashidhar, *Clean: Soil, Air, Water*, 2015, **43**(4), 479–489.
21 F. Yu, Y. Li, S. Han and J. Ma, *Chemosphere*, 2016, **153**, 365–385.
22 S. Wu, X. Zhao, Y. Li, C. Zhao, Q. Du, J. Sun, Y. Wang, X. Peng, Y. Xia and Z. Wang, *Chem. Eng. J.*, 2013, **230**, 389–395.
23 S. P. Sun, T. A. Hatton and T.-S. Chung, *Environ. Sci. Technol.*, 2011, **45**(9), 4003–4009.
24 B. De Witte, J. Dewulf, K. Demeestere and H. V. Langenhove, *J. Hazard. Mater.*, 2009, **161**(1–2), 701–708.
25 B. Li and T. Zhang, *Environ. Sci. Technol.*, 2010, **44**(9), 3468–3473.
26 C. Girardi, J. Greve, M. Lamshöft, I. Fetzer, A. Miltner, A. Schäffer and M. Kästner, *J. Hazard. Mater.*, 2011, **198**, 22–80.
27 Y. Yan, S. Sun, Y. Song, X. Yan, W. Guan, X. Liu and W. Shi, *J. Hazard. Mater.*, 2013, **250–251**, 106–114.
28 F. Yu, J. Ma, J. Wang, M. Z. Zhang and J. Zheng, *Chemosphere*, 2016, **146**, 162–172.
29 F. Yu, J. Ma and D. Bi, *Environ. Sci. Pollut. Res.*, 2015, **22**, 4715–4724.
30 J. Ma, F. Yu, L. Zhou, L. Jin, M. X. Yang, J. S. Luan, Y. H. Tang, H. B. Fan, Z. W. Yuan and J. H. Chen, *ACS Appl. Mater. Interfaces*, 2012, **4**(11), 5749–5760.
31 S. Carabineiro, T. Thavorn-Amornsri, M. Pereira, P. Serp and J. Figueiredo, *Catal. Today*, 2012, **186**(1), 29–34.
32 Z. Pei, X. Q. Shan, J. Kong, B. Wen and G. Owens, *Environ. Sci. Technol.*, 2010, **44**(3), 915–920.
33 C. Gu and K. Karthikeyan, *Environ. Sci. Technol.*, 2005, **39**, 9166–9173.
34 J. Ma, M. Yang, F. Yu and J. Zheng, *Sci. Rep.*, 2015, **5**, 13578.
35 W. M. Algothmi, N. M. Bandaru, Y. Yu, J. G. Shapter and A. V. Ellis, *J. Colloid Interface Sci.*, 2013, **397**, 32–38.
36 E. Abdel-Halim and S. S. Al-Deyab, *Carbohydr. Polym.*, 2011, **84**(1), 454–458.
37 V. Rocher, A. Bee, J.-M. Siaugue and V. Cabuil, *J. Hazard. Mater.*, 2010, **178**(1–3), 434–439.

38 I. M. Diniz, C. Chen, S. Ansari, H. H. Zadeh, M. Moshaverinia, D. Chee, M. M. Marques, S. Shi and A. Moshaverinia, *J. Prosthodontics*, 2016, **25**(2), 105–115.
39 B. Y. Choi, H. J. Park, S. J. Hwang and J. B. Park, *Int. J. Pharm.*, 2002, **239**(1–2), 81–91.
40 E. G. Deze, S. K. Papageorgiou, E. P. Favvas and F. K. Katsaros, *Chem. Eng. J.*, 2012, **209**, 537–546.
41 L. Yin, L. Fei, C. Tang and C. Yin, *Polym. Int.*, 2007, **56**(12), 1563–1571.
42 Y. Zhu, S. Murali, W. Cai, X. Li, J. W. Suk, J. R. Potts and R. S. Ruoff, *Adv. Mater.*, 2010, **22**(35), 3906–3924.
43 F. Fan, C. Luo, M. Sun, X. Li, F. Lu and H. Qiu, *Bioresour. Technol.*, 2012, **114**, 703–706.
44 Y. Lin, S. Xu and J. Li, *Chem. Eng. J.*, 2013, **225**, 679–685.
45 V. Chandra, J. Park, Y. Chun, J. W. Lee, I.-C. Hwang and K. S. Kim, *ACS Nano*, 2010, **4**(7), 3979–3986.
46 V. Chandra and K. S. Kim, *Chem. Commun.*, 2011, **47**, 3942–3944.
47 K.-H. Liao, Y.-S. Lin, C. W. Macosko and C. L. Haynes, *ACS Appl. Mater. Interfaces*, 2011, **3**(7), 2607–2615.
48 M. A. Karim, D. Hossain, M. I. Hossain, S. S. Dipti and M. A. K. Azad, *Water Sci.*, 2024, **38**(1), 109–127.
49 M. A. Karim, M. Najibullah, S. Ahmed, S. S. Dipti and S. M. A. Salam, *Biomass Convers. Biorefin.*, 2025, **15**, 24149–24168.
50 D. Hossain, M. M. H. Prodhan, M. H. Hossain, S. S. Dipti, M. A. K. Azad and M. A. Karim, *Bangladesh J. Sci. Ind. Res.*, 2024, **59**(1), 47–54.
51 B. Aliakbari, S. Amini, H. Ebrahimzadeh and S. H. Kandeh, *Chem. Pap.*, 2023, **77**, 5213–5225.
52 S. Ahmed, D. Hossain, S. S. Dipti, M. A. Karim and M. A. K. Azad, *Sci. Rep.*, 2026, **16**, 1470.
53 Y. Zhuang, F. Yu, J. Ma and J. Chen, *New J. Chem.*, 2015, **39**, 3333–3336.
54 J. W. Choi and S. J. Choi, *Toxics*, 2022, **10**(2), 77.
55 W. Shao, H. Liu, X. Liu, S. Wang and R. Zhang, *RSC Adv.*, 2014, **5**, 4795–4803.
56 F.-T. Zohra, M. A. Swarna and E. Mobin, *Sustainable Chem. Environ.*, 2024, **6**, 100092.
57 P. P. Sharma, V. D. C. Tinh and D. Kim, *Membranes*, 2021, **11**(4), 238.
58 A. Khadir, M. Motamedi, M. Negarestani, M. Sillanpää and M. Sasani, *Int. J. Biol. Macromol.*, 2020, **162**, 663–677.
59 N. Sikri, S. Kumar, B. Behera and J. Mehta, *Front. Nanotechnol.*, 2025, **7**, 1578620.
60 X. Huang, Y. Li, X. Yin and W. Wu, *Langmuir*, 2020, **36**(37), 10895–10904.
61 Y. Yu, G. Zhang and L. Ye, *J. Appl. Polym. Sci.*, 2019, **136**, 47318.
62 M. Rezvani-Ghalhari, R. Nabizadeh, S. M. Alizadeh, D. Sanaei, P. Bashardoust, D. J. McClements, S. Nasseri and A. H. Mahvi, *Int. J. Biol. Macromol.*, 2024, **278**(Pt 3), 134847.
63 W. Ying, T. Yiming, L. Laisheng, L. Peihong, L. Xukai, C. Weirui and X. Ying, *Front. Chem.*, 2018, **6**, 17.
64 M. Laabd, Y. Brahmi, B. El Ibrahimi, A. Hsini, E. M. Toufik, Y. Abdellaoui, H. A. Oualid, M. Ouardi and A. Albourine, *J. Mol. Liq.*, 2021, **338**, 116705.
65 J.-Z. Guo, B. Li, L. Liu and K. Lv, *Chemosphere*, 2014, **111**, 225–231.
66 A. Rahdar, S. Rahdar, S. Ahmadi and J. Fu, *Ecol. Chem. Eng. S*, 2019, **26**(2), 299–311.
67 T. Liu, W. Liu, X. Li, H. Wang, Y. Lan, S. Zhang, Y. Wang and H. Liu, *Sci. Rep.*, 2024, **14**, 19831.
68 X. Xu, J. He, Y. Li, Z. Fang and S. Xu, *Open J. Soil Sci.*, 2014, **4**, 407–416.
69 E.-S. El-Shafey, H. Al-Lawati and A. S. Al-Sumri, *J. Environ. Sci.*, 2012, **24**(9), 1579–1586.
70 N. L. Jorge, M. V. Garrafa, J. M. Romero, M. J. Jorge, L. C. Jorge, M. R. Delfino and Y. V. Meruvia-Rojas, *Molecules*, 2024, **29**, 1760.
71 Z. H. Khudhair and L. S. Jasim, *Syst. Rev. Pharm.*, 2021, **12**(2), 384–393.
72 T. C. Q. Ngo, V. T. Lam, H. T. T. Nguyen, N. B. Hoang, T. T. Tran, M. H. Le, T. N. D. Nguyen and L. G. Bach, *J. Chem. Res.*, 2023, **47**(5), DOI: 10.1177/17475198231184801.
73 B. Gunes, Y. Jaquet, L. Sánchez, R. Pumarino, D. McGlade, B. Quilty, A. Morrissey, Z. Gholamvand, K. Nolan and J. Lawler, *Materials*, 2021, **14**(21), 6343.
74 M. A. A. Aljar, S. Rashdan and A. AbdEl-Fattah, *Polymers*, 2021, **13**, 4000.
75 M. Wahab, M. Zahoor, S. M. Salman, A. W. Kamran, S. Naz, J. Burlakovs, A. Kallistova, N. Pimenov and I. Zekker, *Water*, 2021, **13**, 1969.
76 C. T. Umeh, K. N. John, M. Refilwe, G. A. Kovo and H. O. Nkechi, *Int. J. Phytorem.*, 2024, **26**(10), 1593–1610.
77 C. T. Umeh, A. B. Akinyele, N. H. Okoye, S. S. Emmanuel, K. O. Iwuozor, I. P. Oyekunle, J. O. Ocheje and J. O. Ighalo, *Environ. Nanotechnol., Monit. Manage.*, 2023, **20**, 100891.
78 M. A. Karim, S. Ahmed, D. Hossain, M. I. Hossain, M. S. Hossain, A. Hossain, M. H. Rahman, S. S. Dipti and M. A. K. Azad, *J. Sci. Eng. Pap.*, 2024, **1**(1), 18–25.
79 M. A. Karim, M. S. Sajeeb, S. Chandra and S. S. Dipti, *J. Sci. Eng. Pap.*, 2024, **1**(2), 73–80.
80 Y. Fei, Y. Li, S. Han and J. Ma, *J. Colloid Interface Sci.*, 2016, **484**, 196–204.
81 U. K. Sahu, S. Tripathy, N. Gouda, H. S. Mohanty, B. Dhannjaya, V. K. Choudhury, A. Sahu and A. Gouda, *J. Iran. Chem. Soc.*, 2023, **20**, 2057–2067.
82 R. T. Hanlon, *Found. Chem.*, 2024, **26**, 179–189.
83 Y. Yu, G. Zhang and L. Ye, *J. Appl. Polym. Sci.*, 2019, **136**(14), 47318.
84 B. Wang, Y. Wan, Y. Zheng, X. Lee, T. Liu, Z. Yu, J. Huang, Y. S. Ok, J. Chen and B. Gao, *Crit. Rev. Environ. Sci. Technol.*, 2018, **49**(4), 318–356.
85 C. Liu, H. Liu, T. Xiong, A. Xu, B. Pan and K. Tang, *Polymers*, 2018, **10**(8), 835.